coatings

MDPI

Article

Directional Trans-Planar and Different In-Plane Water Transfer Properties of Composite Structured Bifacial Fabrics Modified by a Facile Three-Step Plasma Treatment

Fengxin Sun [1,2,3], Zhiqiang Chen [1], Licheng Zhu [4], Zhaoqun Du [2], Xungai Wang [1,4] and Maryam Naebe [1,*]

1 Institute for Frontier Materials, Deakin University, Victoria 3216, Australia; 1142007@mail.dhu.edu.cn (F.S.); c.zhiqiang@deakin.edu.au (Z.C.); xungai.wang@deakin.edu.au (X.W.)
2 Key Laboratory of Textile Science & Technology, Ministry of Education, College of Textiles, Donghua University, Shanghai 201620, China; duzq@dhu.edu.cn
3 College of Textiles and Clothing, Jiangnan University, Wuxi 214122, China
4 College of Textile Science and Engineering, Wuhan Textile University, Wuhan 430200, China; lichengz84@sina.com
* Correspondence: maryam.naebe@deakin.edu.au; Tel.: +61-3-5227-2783

Received: 24 July 2017; Accepted: 16 August 2017; Published: 22 August 2017

Abstract: Fabrics with moisture management properties are strongly expected to benefit various potential applications in daily life, industry, medical treatment and protection. Here, a bifacial fabric with dual trans-planar and in-plane liquid moisture management properties was reported. This novel fabric was fabricated to have a knitted structure on one face and a woven structure on the other, contributing to the different in-plane water transfer properties of the fabric. A facile three-step plasma treatment was used to enrich the bifacial fabric with asymmetric wettability and liquid absorbency. The plasma treated bifacial fabric allowed forced water to transfer from the hydrophobic face to hydrophilic face, while it prevented water to spread through the hydrophobic face when water drops were placed on the hydrophilic face. This confirmed one-way water transport capacity of the bifacial fabric. Through the three-step plasma treatment, the fabric surface was coated with a Si-containing thin film. This film contributed to the hydrophobic property, while the physical properties of the fabrics such as stiffness and color were not affected. This novel fabric can potentially be used to design and manufacture functional and smart textiles with tunable moisture transport properties.

Keywords: directional water transport; bifacial fabrics; three-step plasma treatment; composite structure; moisture management

1. Introduction

The biomimetic water transport property of materials has attracted great attention recently [1]. Examples may include the water harvesting materials and microfluidic devices inspired by Stenocara beetle [2], spider silk [3] and cactus [4–6]. Recently, the ability of directional water transport in textile materials has been reported and fabrics with multi dimension liquid moisture transport properties are of great potential for technical and smart textiles. Such fabrics have a broad spectrum of end uses e.g., filters, desalination, composite and sportswear [7–10].

Until now, two main approaches, constructing the hydrophobicity-to-hydrophilicity gradients of fibrous layers across fabric thickness and building asymmetric hydrophilicity of fabric surfaces, have been developed to create surface energy gradients along the thickness of textile fabrics and to achieve directional water transfer properties. In the case of the first method, Wang et al. [11] reported

a special coating technique that formed a wettability gradient through the fabric thickness and created a fabric with directional water-transport properties. Zhang et al. [12] used a phase segregation method in the formation of a hydrophilic-to-hydrophobic gradient membrane to achieve directional water transport. Wu et al. [13] also combined a hydrophobic film and a hydrophilic film seamlessly and developed a unidirectional water-penetration nanofiber membrane. Fabric with asymmetric wettability by surface modification also showed directional water transfer effect. In this case, the micro-processing techniques used for producing rough surface, such as plasma etching [14–16], and chemical treatment with fluoro-containing monomer or silicon polymers for reducing the surface free energy [17–19], as well as other methods, such as sol-gel process [20,21], electrospinning [22,23], self-assembly [24] and spray coating [25], were used to create a hydrophobic surface in textile fabrics, forming water pressure differentials between two surfaces of the fabric. For example, Tian et al. [26] used a vapor-phase method to deposit a fluoroalkylsilane on one side of cotton fabric to create directional gating of droplets in air-water system. Zeng et al. [27] prepared a one-way water transport fabric by electro-spraying a hydrophobic layer on one side of the fabric. However, most of the current studies only focused on the trans-planar water transport of textile materials, and little research is reported on both trans-planar and in-plane water transport properties.

Plasma treatment is gaining favor for its environment friendly and energy efficient characteristics [28–30]. It has been found that plasma polymerization was the effective approach for preparing directional moisture transfer fabrics. Recently, some works have shown that the fabrics became hydrophobic after plasma polymerization of hexamethyldisiloxane (ppHMDSO) [31–33]. However, the studies only qualitatively analyzed the moisture transfer property, and quantitative evaluation has received little attention. Therefore, it is difficult to evaluate the moisture transfer performance of treated fabrics to determine their practical applications. In addition, in the past only transplanar water transport properties of fabrics were analyzed and in-plane water transport properties have not been the focus of these studies.

Our group has reported on the design and manufacturing a novel composite structured bifacial fabric with a knitted structure on one face and a woven structure on the other [34]. The bifacial fabric showed different in-plane moisture transfer properties on its two faces, indicating the potential of the bifacial fabric as moisture management materials [35,36]. In this paper, a study was reported on the use of a three-step plasma treatment to create asymmetric wettability on two faces of the fabric for development of a directional water transport fabric. A quantitative investigation into the transplanar and different in-plane moisture transfer properties of the treated samples was carried out by using the Moisture Management Tester (MMT). Studies of the surface chemistry and morphology as well as the stiffness and color of the treated fabrics were also conducted to analyze the mechanism and characteristics of the water management ability of the bifacial fabric.

2. Experimental Details

2.1. Materials

The details of the bifacial fabric (combination of a plain weave and a single jersey) and the corresponding woven (plain weave) and knitted (single jersey) fabrics have been described before [36], and are briefly summarized in Table 1. The cross-section of bifacial fabric in the warp direction and its appearances on the two faces are illustrated in Figure 1. The bifacial fabric was manufactured on a purpose-built machine which incorporated a flat knitting bed into a sample rapier loom. The woven and knitted fabrics as control samples were fabricated on a weaving machine (CCI, Taipei, Taiwan) and a knitting machine (Shima Seiki SES, Wakayama, Japan), respectively. The warp yarns (set of yarn running lengthwise—machine direction) in these fabrics were pure polyester staple yarns, while both the weft yarns (transverse thread in a direction perpendicular to machine direction) and knitted loop yarns were made of 65/35 wool/acrylic fibers. All the fabrics were cleaned with acetone and ethanol and rinsed with deionized water, and then were dried under the fume hood before plasma treatment.

Argon gas (purity 99.99%), O_2 gas (purity 99.99%) and HMDSO (hexamethyldisiloxane; purity 99.5%; Sigma Aldrich, St. Louis, MO, USA) were used as the plasma reactor reagents.

Table 1. The details of the fabric substrates.

Fabric	Warp Yarns		Weft/Loop Yarns		Loop Length (mm)	Weft Density (Picks/cm)
	Material	Count (tex)	Material	Count (tex)		
Woven	100% polyester	56	35% acrylic/65% wool	65	N/A	22
Knitted	N/A	–	35% acrylic/65% wool	65	11	N/A
Bifacial	100% polyester	56	35% acrylic/65% wool	65	11	22

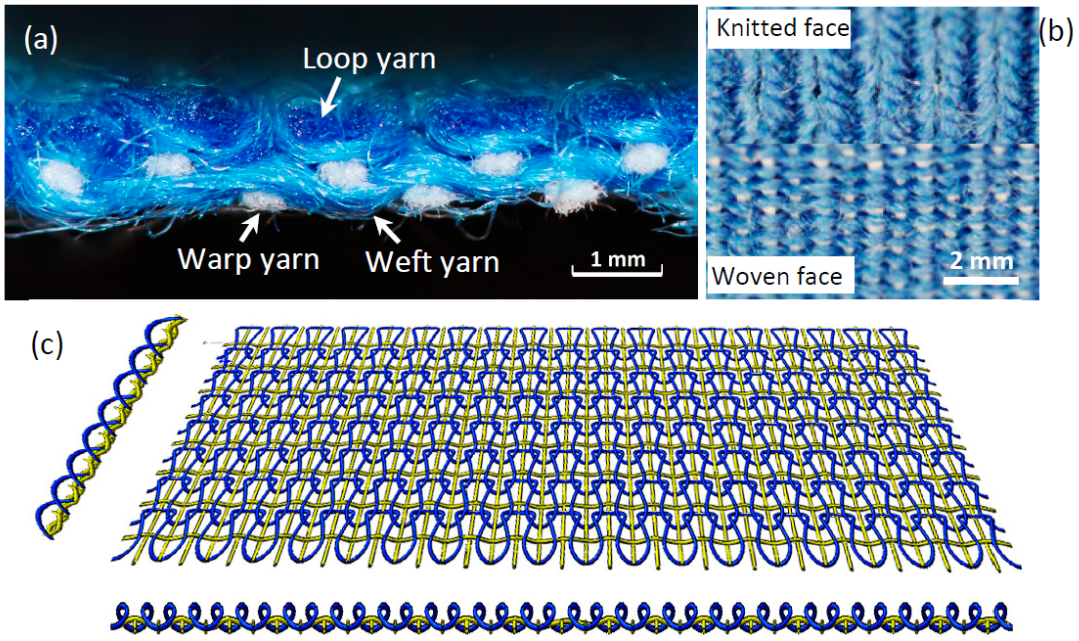

Figure 1. Bifacial fabric (**a**) the cross-section in the warp direction; (**b**) knitted (top) and woven (bottom) face; (**c**) schematic structure.

2.2. Plasma Treatment

The three-step plasma treatment method used for surface modification of fabrics included (Figure 2a) (1) argon plasma activation to form clean and activated fabric surface, (2) subsequent oxygen plasma functionalization to introduce oxygen functional groups on the fabric surface [37,38], and (3) then followed by plasma polymerization of HMDSO as the third and final step. The plasma process was performed in a cylindrical glass reactor with an external antenna around the chamber and a stainless steel as a sample holder in the middle of the reactor (Figure 2b). A radio frequency generator was used to generate the plasma, which can be operated in a continuous wave mode or a pulsed mode [39].

In the treating process, a 9 cm × 9 cm sample was placed on the sample holder with the treatment surface up, while the base pressure lower than 1×10^{-3} mbar was achieved with a rotary pump. Then the continuous wave argon plasma was used to pretreat the samples at a stable pressure of 2.8×10^{-2} mbar with a radio frequency power of 100 W for 2 min. After the activation process, the oxygen plasma was applied (100 W, 3.5×10^{-2} mbar) at a pulsed mode of 20% duty cycle for 2 min. Subsequently, the HMDSO vapor was supplied at a pulsed mode of 10% duty cycle with a power of 100 W for 3 min under the pressure of 1.0×10^{-1} mbar. The duty cycle is defined as ton/(ton + toff) × 100% [38], where ton and toff are the time that the plasma is "on" and "off", respectively.

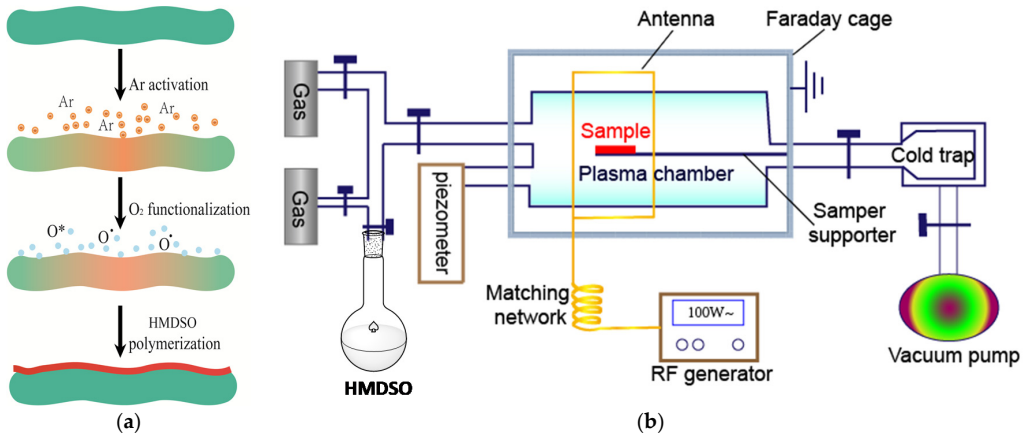

Figure 2. Schematic of (**a**) the three-step plasma treatment and (**b**) the plasma device.

2.3. Contact Angle and MMT Test

The treated fabrics were conditioned in the condition room (20 ± 2 °C and 65 ± 2% relative humidity) for 24 h prior to the characterizations. The water contact angle (CA) and absorption time were measured in the condition room by a KSV CAM 200 contact angle meter (KSV Instruments Ltd., Helsinki, Finland). Water droplets with a volume of 5 µL were placed on the surface of the sample that was pasted on a slide glass and placed on the sample stage. The average of five measurements was reported for each sample.

The moisture transfer property was measured by the Moisture Management Tester (MMT; SDL Atlas, Rock Hill, SC, USA) according to the AATCC Test Method 195-2011. The saline water (0.22 cm^3; containing 0.9% NaCl to simulate sweat) was introduced in 20 s onto the upper surface of the fabric, and the spread and content (in the first 120 s since starting pumping the water) of the saline water on both faces of the fabric sample were recorded by the sensors touching the upper and lower surfaces of the fabric.

2.4. Scanning Electron Microscopy (SEM)

The surface morphology of the coated and uncoated face of fabrics was observed by environment scanning electron microscopy (SEM, Quanta-250, FEI, Brno, Czech) operated at 5 kV accelerating voltage.

2.5. Fourier Transform Infrared Spectroscopy (FTIR)

FTIR-ATR spectroscopy was used to analyze the chemical composition and functional groups on the surface of the fabrics. Infrared spectra were recorded with a NICOLET 5700 instrument (Thermo Nicolet Instrument Company, Madison, WI, USA) in attenuated total reflectance (ATR) mode with an accumulation of 64 scans at 4 cm^{-1} resolution. The spectra of treated and untreated samples were recorded for comparison.

2.6. X-ray Photoelectron Spectroscopy (XPS)

XPS spectra was carried out on the HMDSO plasma polymer coated on a silicon slice by the three-step plasma. XPS analysis used a K-Alpha X-ray photoelectron spectrometer from Thermo Fisher Scientific, Waltham, MA, USA. A spot size of 400 µm was used to scan in the region of the C1s binding energy as well as provide a broad survey spectrum to detect additional elements. Excessive charging of the samples was minimized using a flood gun. The C1s binding energies of the poly(HMDSO) were accurately established by charge shift correcting the lowest binding energy peak of the C1s to 284.6 eV. The survey spectra were obtained at a pass energy of 100 eV while high resolution peak scans were performed at a 20 eV pass energy. The peak scans were used to obtain the elemental composition of C, Si and O. Triplicate samples were analyzed with atom percent uncertainties being of the order of 2%.

2.7. Handle Characteristics and Appearance

Handle characteristic of fabrics was evaluated using a Comprehensive Handle Evaluation System for Fabrics and Yarns (CHES-FY; see Figure 3) developed by Donghua University (Shanghai, China) [40,41]. The CHES-FY simultaneously measures multiple low stress mechanical properties of fabric by a pulling-out test and assesses fabric's stiffness handle. During the testing, a hanging fabric strip of 180 mm × 20 mm in warp × weft direction is pulled by a pulling pin with diameter of 2 mm through a space distance between bi-U-shaped pins, constructing a complex deformation of the fabric. The pulling-out force during the process is recorded by the force sensor connecting to the pulling pin. The average of three pulling-out force—displacement curves and the corresponding stiffness handle attribute were reported for each sample.

The effect of plasma treatment on fabric appearance was evaluated using colorimeter (SC-10 3NH, Shenzhen, China). The fabric's chromatic aberration (ΔE) after treatment is expressed as,

$$\Delta E = \sqrt{(\Delta L)^2 + (\Delta a)^2 + (\Delta b)^2} \quad (1)$$

where ΔL, Δa and Δb represent the changes of lightness/darkness, red/green chroma and yellow/blue chroma after plasma, respectively.

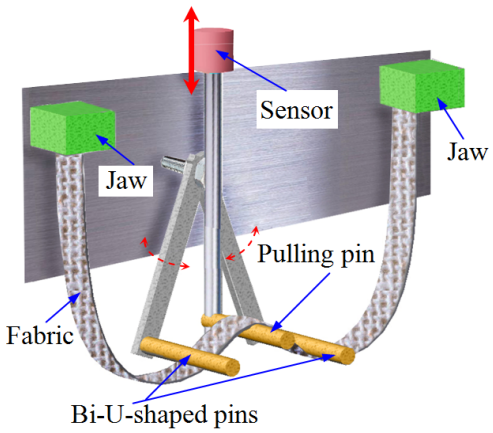

Figure 3. The schematic structure of the Comprehensive Handle Evaluation System for Fabrics and Yarns (CHES-FY).

2.8. Statistical Analysis

To study the effect of the plasma treatment on the curve parameters and handle stiffness characteristic of fabrics, the *t*-test was used to analyze the differences between the treated and untreated samples based on a *p*-value = 0.05. The *p*-value is the estimated probability of rejecting the null hypothesis when there is no difference between treatments.

3. Results and Discussion

3.1. Fabrics with Asymmetric Wettability by Plasmas

Figure 4 shows the effect of coating time on the contact angle of the coated face and on absorption time of the opposite face (uncoated face) when water droplets (5 μL) are placed on the surface of the bifacial fabric. The optimum asymmetric wettability of the bifacial fabric takes place when the coating time is around 3 min. The contact angle of the coated face has little increase when the coating time is longer than 3 min, while water absorption time of uncoated face increases dramatically, which may due to permeation of the HMDSO polymerization. An example of the asymmetric wetting performance of bifacial fabrics with three-step plasma treatment of 3 min coating period is illustrated in Figure 4b.

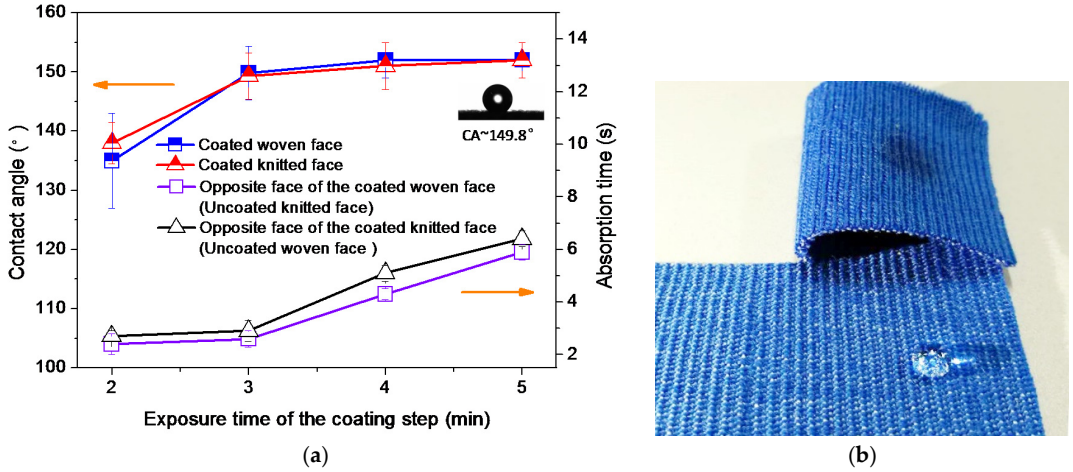

Figure 4. Water contact and absorption properties of bifacial fabric (**a**) effect of coating time on contact angle (CA) of the coated face and absorption time of uncoated face, error bars indicate standard deviation. Note the two different *y*-axis scales. (**b**) A hydrophobic woven face (coated) and a hydrophilic knitted face (uncoated).

Since the optimum asymmetric wettability of the bifacial fabric was achieved with 3 min plasma coating, further experiments and analysis were carried out using the 3 min coating. The contact angle and absorption time results before and after plasma treatment of bifacial fabric and woven and knitted fabrics (control samples) are summarized in Table 2. The contact angle and absorption time of the bifacial, woven and knitted fabrics considerably increased after plasma treatment ($p < 0.01$ based on a one-way analysis of variance), and the fabrics showed similar hydrophobicity on the coated face after the treatment, as indicated by the contact angles of the coated face for all fabrics being close to 150° and absorption time higher than 40 min. However, the uncoated face of all fabrics retained its wettability and more interestingly showed a shorter absorption time after plasma treatment compared with the one before treatment. This could be mainly attributed to the activation and partial oxidation of the plasma treated surface using argon and then oxygen. It has been shown that plasma treatment using inorganic gas (such as argon, helium and oxygen) introduced new active sites on the surface and etched the fibre surface of the polyester and acrylic [42,43]. For wool fibres, partial removal of lipid layer and formation of cysteic acid after plasma was reported, which confers surface wettability and enhances the wicking properties of the fabrics [28,44,45]. Although sampling issues and visualisation of thin polymer films deposited on fibres using scanning electron microscopy are problematic, there was some evidence to suggest that silicon polymer is formed only on the fibre surface of the coated face (hydrophobic face). An example is shown in Figure 5, where both uncoated and coated faces of the plasma treated bifacial fabric can be observed. The images also show some physical modifications such as smoothening of the scale edges on the wool fibres after plasma treatment. The results confirm the feasibility of three-step plasma treatment to create asymmetric wettability of fabrics by the surface-specific coating.

The FTIR results in Figure 6A show bifacial fabric's surface chemistry produced by the three-step plasma treatment. The distinct absorption peak at 1110 cm^{-1} is attributed to the stretching vibration of asymmetric Si–O–C bond in the HMDSO plasma polymer of the treated surface of bifacial fabrics, and this peak is found to be much broad, which can be explained by the overlap of Si–O stretching in Si–O–Si bond and Si–O–C stretching at 990–1090 cm^{-1} as well as the asymmetric stretching of S=O (around 1120 cm^{-1}) bond possibly resulting from oxidized disulphide bonds of wool fibre in the oxygen plasma step [46–48]. Another new absorption peak in the FTIR spectra of the treated fabric emerged at 810 cm^{-1} compared to that of the untreated fabric, corresponding to Si–C stretching. However, inherent peaks of the wool/acrylic bifacial fabric were decreased after the plasma treatment. The peak attributed to C–N–H bonding deformation around 1520 cm^{-1} observably decreased compared to the untreated fabric [49], and the peak at 1690 cm^{-1} corresponding to C=O stretching in –COOH

functional group also became flat after the treatment [50]. This can be attributed to the removal of the covalently-bound fatty acid layer (F-layer) from the surface of the wool fibres, resulting in exposure of the underlying, hydrophilic protein material [45]. To further determine surface atomic composition after the treatment, XPS spectra was carried out on the HMDSO plasma polymer coated on a silicon slice by the three-step plasma. From Figure 6B, it can be seen that plasma coatings contain carbon, oxygen and silicon, which are the constituent elements of the Si-containing monomer. The Si2p spectra of the plasma coatings can be decomposed into three components at 100.8 eV, 101.8 eV and 102.4 eV, corresponding to Si–O–Si, Si–C and Si–O–C, respectively [51,52]. This reaffirms the generation of Si-containing monomers that detected by the FTIR, and these silicon compounds contribute to the hydrophobic surface of the samples [53].

Table 2. Comparisons of the contact angle (CA) and absorption time (AT) before and after 3 steps plasma treatment.

Sample	Without Plasma [35]		After Plasma			
			Coated Face		Uncoated Face	
	CA (° ± SD [a])	AT (s)	CA (° ± SD)	AT (s)	CA (° ± SD)	AT (s)
Bifacial fabric woven face	122.1 ± 2.9	>120	149.8 ± 4.5	>2400	wets	<3
Bifacial fabric knitted face	125.8 ± 4.7	>120	149.3 ± 3.9	>2400	wets	<3
Woven fabric	120.0 ± 9.0	30	150.0 ± 2.9	>2400	wets	<4
Knitted fabric	124.3 ± 3.5	>120	147.1 ± 4.8	>2400	wets	<3

[a] Standard deviation of five measurements.

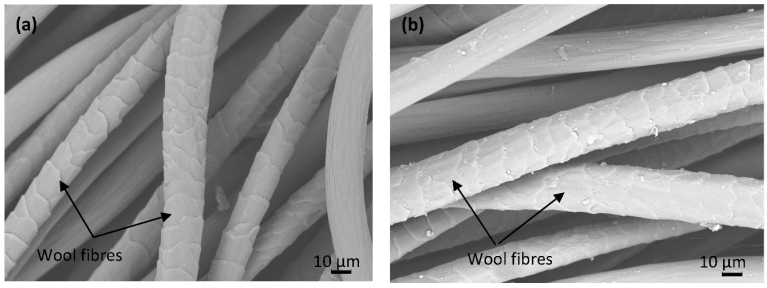

Figure 5. SEM images of the (**a**) uncoated face and (**b**) coated face of the bifacial fabrics after three-step plasma treatment.

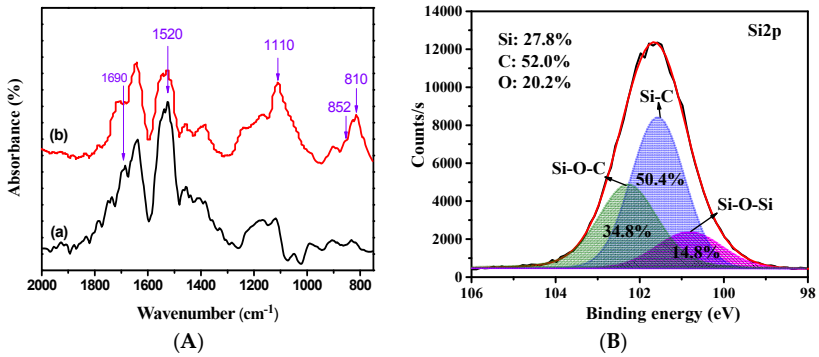

Figure 6. (**A**) FTIR spectra of the bifacial fabric: (a) untreated and (b) plasma treated; (**B**) XPS Si2p spectra of HMDSO plasma polymer.

3.2. Moisture Management Properties

3.2.1. Typical Relative Water Content Curves of the Fabrics

The typical MMT relative water content curves of the upper and bottom surfaces for bifacial fabrics are shown in Figure 7, where Figure 7a,b shows the water content on the bifacial fabrics with poly(HMDSO) coated knitted and woven faces down on the MMT, respectively. Regardless of woven or knitted structures, by just comparing the water content curves of the coated and uncoated faces in Figure 7a,b, it was found that the water content of the uncoated faces increased dramatically and then rapidly spreads; the content exceeded 600% in 20 s. However, the water content on the coated faces slowly increased and then stayed at low percentage around 100%. By focusing on water content on the reverse structures of the fabric placed on the MMT (Figure 7a,b), it was found that the water content of the coated woven face took longer time to increase compared to than that of the coated knitted face. This is probably due to the open structure of the knitted face providing more spaces between loop yarns, resulting in a relatively high water-retaining capacity of the knitted face of bifacial fabrics than woven face. Fabric porosity and distribution of pore connection also play key roles in water content and water retain ability of fabric. Our previous investigation regarding the pore diameter distribution of woven and knitted structure of bifacial fabrics has shown that while woven structure of bifacial fabric has more pore connections, knitted structure has more pores that are larger in size compared to woven structure [36]. It was found that there are more connections around the positions where there are the least number of big pores and the most number of small pores [36]. More connections and small pores in woven structure of bifacial fabric may tend to be blocked by silicone monomer quicker and easier. Therefore, the penetration of water from coated woven side of bifacial fabric will be much slower than the opposite side.

When water was dropped on the coated knitted face (see Figure 7c) and coated woven face (see Figure 7d) of the bifacial fabric, the water content of the upper face coated with poly(HMDSO) presented an small increase and then remained stable at a low level (around 50%), but the uncoated face down showed a sharp increase to around 400%. This implies that the water from the coated face penetrates through the fabric thickness and then spreads into the uncoated face, regardless of the woven and knitted structures. This is not similar to the case when a small water droplet is dropped on the coated face of a fabric in the CA test, because more saline water (0.22 cm^3) was puffed onto fabric's surface, vividly simulating a forced water flow in the MMT test. In addition, unexpected high water content on the coated face was measured by the MMT. This is due to the measurement method where the sensor of MMT slightly penetrates into the fabric (depth around 60 μm [27]), therefore, the water content measured actually reflects the water content in the surface layer around 60 μm.

For comparison purposes, the conventional woven and knitted fabrics (the plain weave and single jersey, see Table 1) were also treated with three-step plasma treatment. Their typical water content curves are illustrated in Figure 8. Unlike bifacial fabric, once the water was dropped on the surface of woven fabric, the water content of both coated and uncoated faces of the fabric increased (Figure 8a,b), and then remained stable with little change after reaching a maximum. This can be explained by the relatively low water absorption and high water spreading property of the woven fabric [35]. Moreover, the water content of the coated face of the woven fabric (Figure 8a) is higher than the coated face of the bifacial fabric (see Figure 7) and it is almost half of the uncoated face, no matter which face is down or up on the MMT (Figure 8a,b). The knitted fabric showed a similar trend to the woven fabric, but presented lower water content on the coated face of the knitted fabric. The decrease of water content after reaching the maximum is more similar to the bifacial fabrics and may be attributed to the relatively high capacity of water conservation of knitted fabrics.

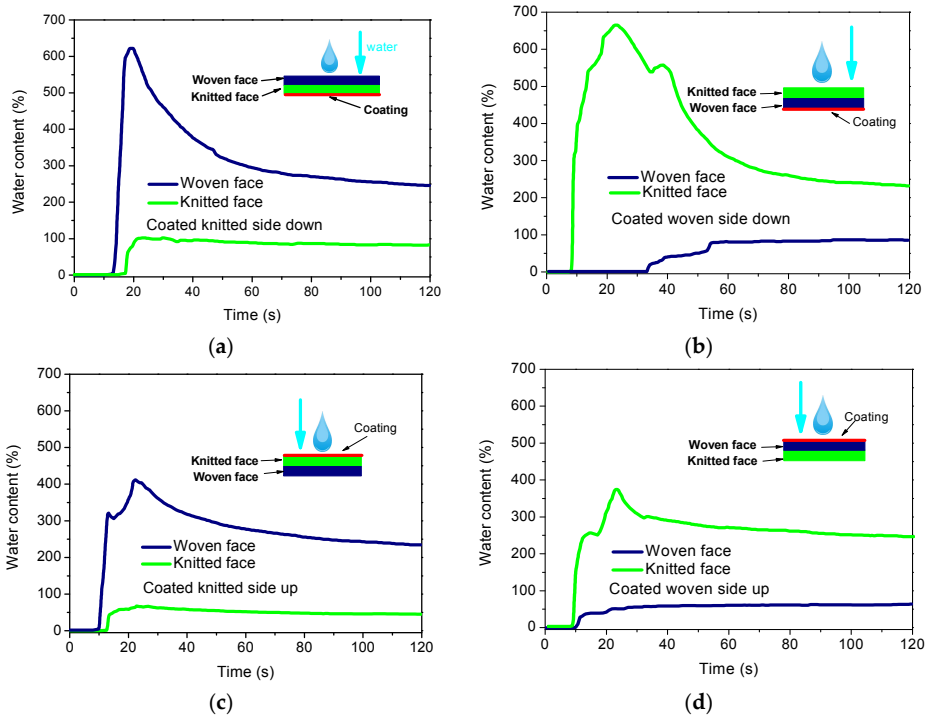

Figure 7. Typical MMT water content curves of bifacial fabrics by dropping water on (**a**) the woven face; (**b**) the knitted face with the coated face down on the MMT; (**c**) the knitted face; (**d**) the woven face with the coated woven face up on the MMT.

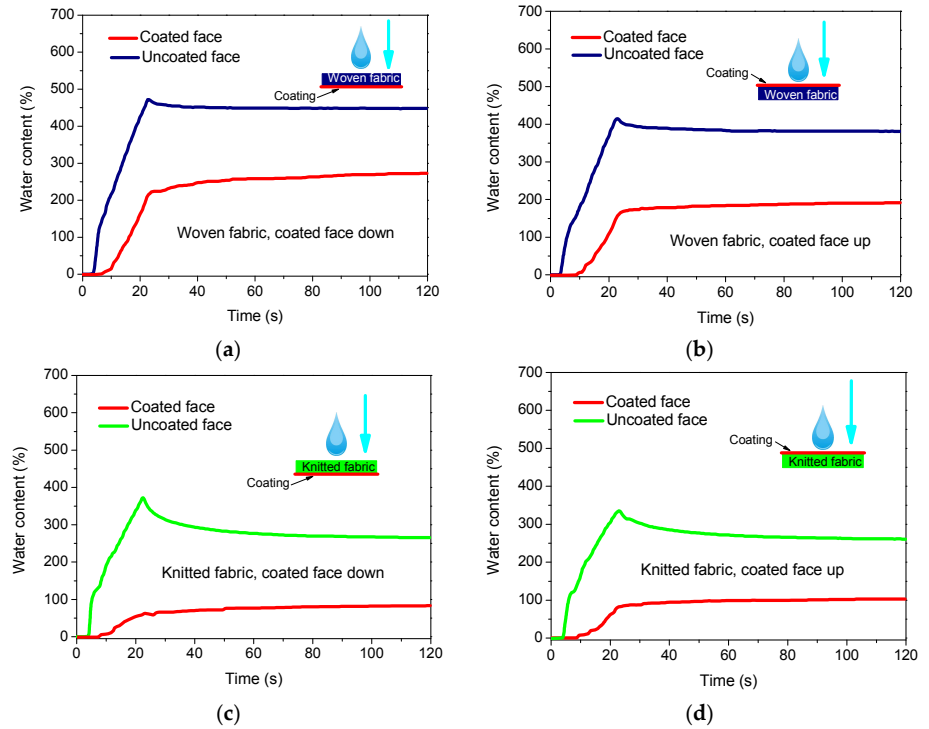

Figure 8. Typical MMT water content curves of (**a**,**b**) knitted fabrics and (**c**,**d**) woven fabrics with the red line presenting the coated face.

3.2.2. Analysis of the Indices from the MMT

A series of indices, including wetting time (WT), maximum absorption rate (MAR), spreading speed (SS) and cumulative one-way transport capacity (OWTC), for evaluating the moisture management properties was derived from MMT (see the definitions of the indices in reference [54]). For convenience, we denoted the fabric samples treated and measured in different conditions by "variety-coated face-direction of coated face". For example, "bi-wc-cd" represents a bifacial fabric (bi) for which the woven face is coated (wc) and the coated face is placed down (cd) in the MMT; "k-cu" means a knitted fabric is tested with the coated face up in the MMT, and so on.

Figure 9a shows the WT (the time period in which fabric surface starts to be wetted) of bifacial, knitted and woven fabrics with the coated face down in the MMT. The WTs of top and bottom faces for bifacial fabrics were all higher than those of conventional knitted and woven fabrics. The WT of the bottom for bi-wc-cd fabric showed a significantly high value, indicating a hydrophobic surface of the coated woven face of the bifacial fabric with low wetting time. This also implies that the knitted face has better water-retaining capacity than woven face of the bifacial fabrics. Figure 9b illustrates the WT with the coated face up in the MMT. It is seen that the bifacial fabric with either coated knitted face up or with coated woven face up and knitted and woven fabrics with the coated face up have similar WT, respectively. However, the WTs of both faces of the bifacial fabric are higher than that of both knitted and woven fabrics, which is due to the larger inter-yarn spaces inside the bifacial fabric absorbing a large amount of water [55,56].

It is observed (Figure 9c,d) that the uncoated woven face of the bifacial fabric has the highest MAR (the initial slope of water content curve), indicating a rapid water spreading on the woven face, in agreement with previous studies [35], but the knitted face reflected a lower MAR than the woven face by comparing the first and third columns of Figure 9c, which actually implies that more water is absorbed by the knitted structure instead of spreading on the knitted surface according to the measurement principle of the MMT [52,57]. Therefore, the knitted surface can be more suitable to improve the transportation of liquids by rapid absorption of water into the fabric, whereas the woven face shows outstanding water spreading behavior along its in-plane direction. Figure 9e,f shows the SS (speed of water spreading on the surface) of the moisture on the top and bottom surfaces of fabrics. The SS of the bifacial fabric is lower than that of the woven and knitted fabric. The greater thickness and larger inter-yarn spaces inside the bifacial fabric absorbing a large amount of water could be a reason for this result. This also can be explained by OWTC, a cumulative moisture content difference between the two surfaces of the fabric (i.e., one-way transport capacity) calculated by the equation [54].

$$\mathrm{OWTC} = \frac{\int_0^T U_b \mathrm{d}t - \int_0^T U_t \mathrm{d}t}{T} \quad (2)$$

where U_b and U_t are the relative water content (%) of the bottom and top layers of the fabric in the MMT, respectively, and T is the total testing time (s).

For common fabrics with isotropic wettability, the water content is similar on two fabric surfaces leading to near zero value of the OWTC, and the OWTC value is similar when the water is dropped on any face of the fabrics. However, the bifacial fabric with coated face up showed the values higher than 173 and 115 for the case of knitted and woven face up in the MMT, respectively, while the OWTC values were about −216 and −289 by placing the coated knitted face down and coated woven face down, respectively (see Table 3). The much greater value than zero and such a large difference between the conditions of coated face up and coated face down in the MMT testing further demonstrated that water tends to transfer from the coated face to uncoated face no matter on which face water is dropped on. This property can be used for different applications; e.g., in clothing the bifacial fabric with coated knitted face next to skin may show a better capacity to transfer the sweat away from the body, as indicated by the high OWTC as 173, whereas the bifacial fabric with coated woven face at the

outer layer would lead to a high resistance to water transport (OWTC = −289), creating dampness discomfort for wearers.

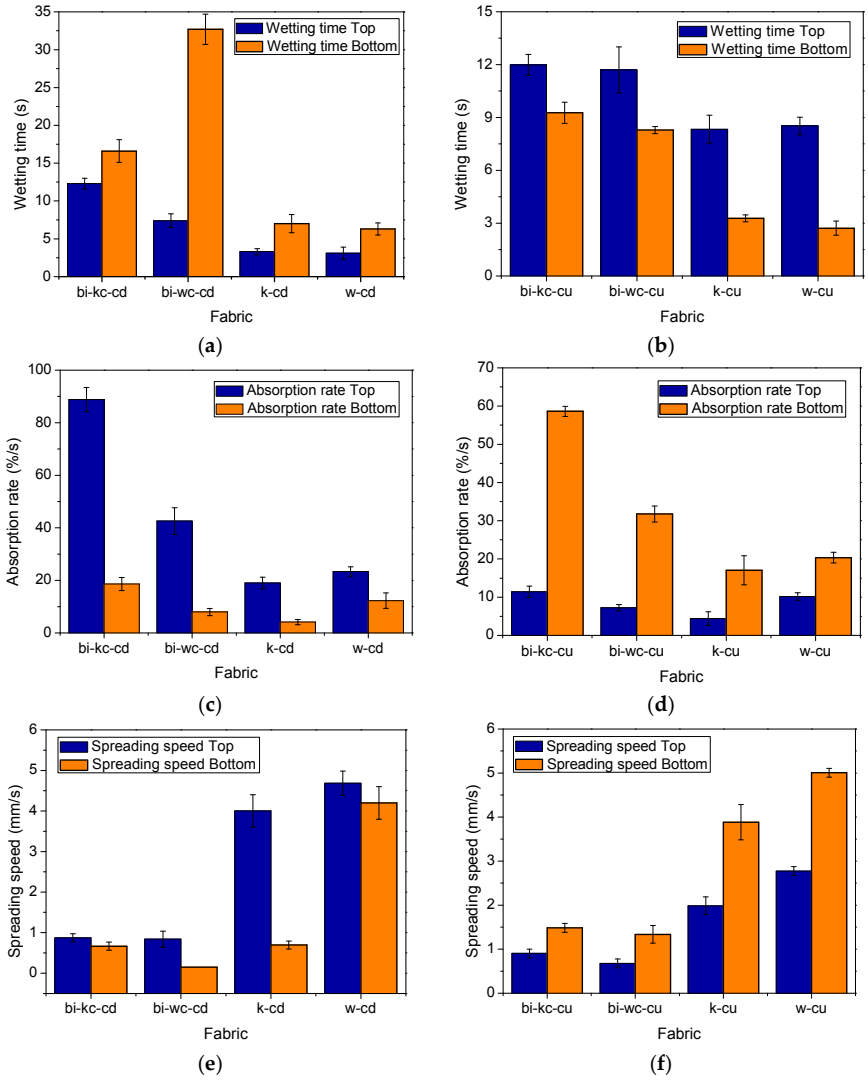

Figure 9. Comparisons of different fabrics by the MMT indices: (**a**,**b**) wetting time; (**c**,**d**) maximum absorption rate; (**e**,**f**) spreading speed. The 'Top' means the upper face of the sample in the MMT, and the 'Bottom' means the lower face of the sample in the MMT.

Table 3. The one-way transport capacity (OWTC, %) results in value of fabric samples.

Fabric Sample	Dropping from Coated Face	Dropping from Uncoated Face
Bifacial fabric with woven face up	115.2	−216.1
Bifacial fabric with knitted face up	173.4	−289.4

Combining the results from MMT, the possible water transfer mechanism of the treated bifacial fabrics is shown in Figure 10. When dropped on the uncoated face, water is absorbed by the hydrophilic matrix and then is blocked when it reaches the coated hydrophobic layer. However, water can permeate across the hydrophobic matrix then into the hydrophilic matrix when it is dropped on the coated face. Also the open structure of the knitted face allows more water to be absorbed, while capillary effect along the warp and weft yarns in the woven structure may provide a shortcut for liquids to spread along the woven face.

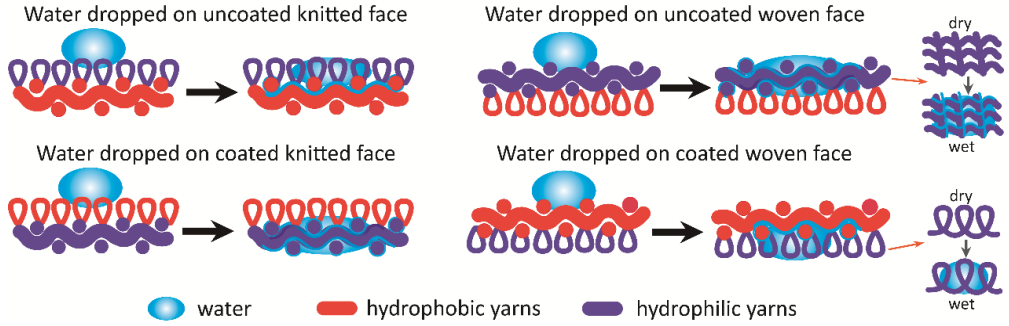

Figure 10. Schematic illustration of a possible mechanism of transplanar (between hydrophobic face and hydrophilic face) and in-plane (on woven face and knitted face) water transport of the treated bifacial fabrics.

3.2.3. Handle Stiffness and Color Evaluation

The stiffness of bifacial, woven and knitted fabrics before and after plasma treatment were evaluated by the CHES-FY. The schematic structure of the CHES-FY and the pulling-out force—displacement curves corresponding to fabric's bending deformation stage are illustrated in Figure 11. The curve parameters, including maximum bending force (P), bending work (A_b), bending slope (K_b), friction work (A_f) and average friction force (U), extracted from the testing curves (see the definition of the curve parameters in [49]) and the grading values of the stiffness handle calculated by the built-in fuzzy comprehensive prediction models of the CHES-FY were also reported [58], and the results are listed in Table 4. The differences of the curve parameters and stiffness handle between the treated and untreated samples were determined using t-test based on a p-value > 0.05 for rejecting the null hypothesis when there is no difference between treatments, which is also included in Table 4.

Table 4. The curve parameters and stiffness handle (ST) of the treated and untreated fabrics, as well as the p-values for judging the differences between the treatments.

Treatment	Sample	A_b (cN·mm)	A_f (cN·mm)	K_b (cN/mm)	K_f (cN/mm)	P (cN)	U (cN)	ST
Treated	Woven fabric	20.7	30.4	0.94	−0.51	5.8	0.69	0.00
	Knitted fabric	31.2	33.5	0.91	−0.57	7.0	1.20	0.01
	Bifacial fabric knitted face	174.2	213.9	5.20	−3.21	39.5	7.34	0.97
	Bifacial fabric woven face	156.2	211.4	5.12	−2.20	37.2	8.50	0.95
Untreated	Woven fabric	16.5	25.5	0.75	−0.37	4.6	0.60	0.00
	Knitted fabric	23.0	32.4	0.91	−0.47	6.0	1.00	0.00
	Bifacial fabric knitted face	144.4	190.7	5.21	−1.97	36.2	7.29	0.93
	Bifacial fabric woven face	150.4	166.4	4.36	−2.39	33.7	6.50	0.89
Untreated—Treated Mean difference	p-value	0.83	0.92	0.90	0.78	0.86	0.88	0.94

Note: A_b, bending work; A_f, friction work; K_b, bending slope; K_f, friction slope; P, maximum bending force; U, average friction force.

Combining the results from Figure 11 and Table 4, it can be concluded that the plasma treatment did not have significant effects on the curve parameters and the stiffness handle of woven, knitted and bifacial fabrics as assessed by the CHES-FY (p-value higher than 0.78), although the curve parameters and the stiffness handle of the treated fabrics in general were slightly higher than that untreated fabrics. This can be due to the etching effect of Ar and O_2 plasma on the surface of the fabrics (Figure 5) [59], while the short exposure time of Ar and O_2 plasma (2 min) and gentle O_2 plasma treatments (pulsed mode of 20% duty) did not result in large impairment of fabric handle. In addition, while HMDSO coating provides a very thin spotted polymer on the surface of the fabric, the polymerization step

may cover some of the surface flaws of the fabrics (Figure 5), results in insignificant changes of the handle attribute.

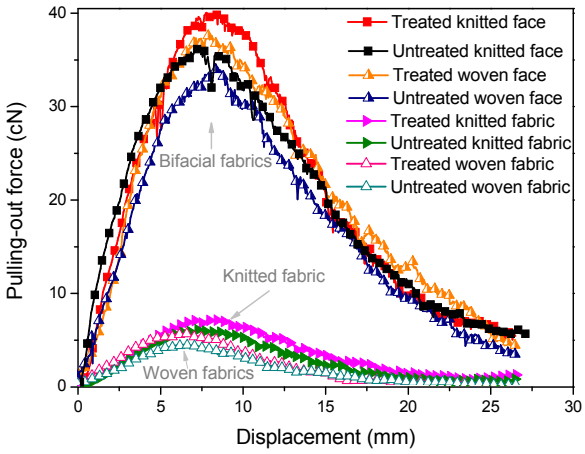

Figure 11. The pulling-out force—displacement curves when the fabrics are bending and sliding on the surface of the bi-U-shaped pins under the pulling action of the pulling pin.

The effect of plasma on fabric's appearance was evaluated by comparing fabric's color before and after plasma treatment. The photos of the fabrics are given in Figure 12A, and the chromatic aberrations (ΔE) of the fabrics before and after treatment are illustrated in Figure 12B. It can be seen that there is no significant differences between untreated and plasma treated fabrics. The relatively small ΔE with the maximum value less than 2.5 indicates that three-step plasma treatment does not change the fabric's color. This confirms that the three-step plasma treatment is gentle and thus has little effect on the surface macro stiffness and appearance of the fabrics.

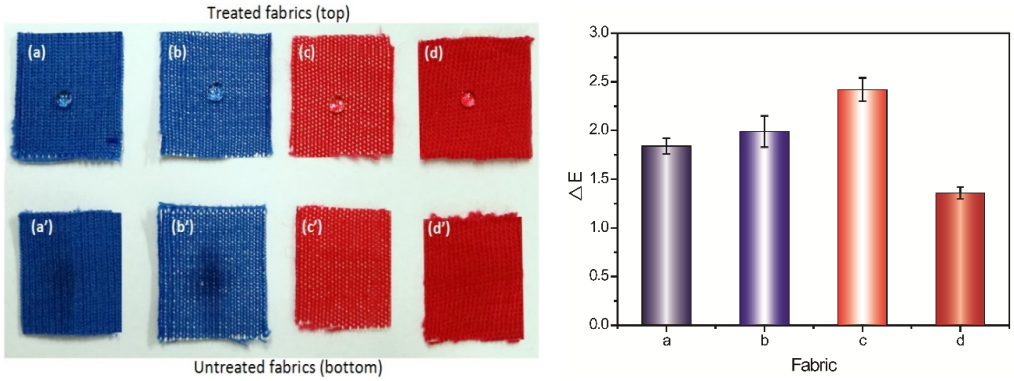

Figure 12. (**A**) Photos of the (a) knitted face of the bifacial fabric, (b) woven face of the bifacial fabric, (c) woven fabric and (d) knitted fabric with the treated samples at the top and untreated samples at the bottom; (**B**) the colour variations (ΔE) of the fabrics before and after plasma treatment.

4. Conclusions

A composite structured bifacial fabric of symmetric wettability, transplanar liquid moisture transfer property and different in-plane water transfer property on two faces was created in this study. It also proved that the three-step plasma treatment was an effective method to induce directional moisture transfer property across thickness of fabrics by combining hydrophobic and hydrophilic faces, while the treated bifacial fabrics still maintained the good water-retaining property on the knitted face, and rapid water spreading performance along the warp and weft direction of the woven face.

Comparing the treated and untreated fabric samples, the gentle and moderate three-step plasma treatment showed little effect on the stiffness and color of fabrics. As confirmed by FTIR-ATR and XPS results and SEM observation, the Si-containing plasma coating contributed to the hydrophobic surface of the samples. Such a novel fabric of directional transplanar moisture transport properties and different in-plane water transfer properties on two faces can be used to engineer the performance of textiles with tunable multifunctional properties. Further studies of the vapour transfer properties of the bifacial fabric would be meaningful and beneficial for the application in clothing.

Acknowledgments: This work was supported by National Natural Science Foundation of China projects (Grant 11272086 and 51203022), the Fundamental Research Funds for the Central Universities (2232014A3-02 and CUSF-DH-D-2016006), Fujian Provincial Key Laboratory of Textiles Inspection Technology (Fujian Fiber Inspection Bureau) of China (2016-MXJ-02), and Fok Ying Tung (huoyingdong) Education Foundation (151071). The authors are grateful to the China scholarship council (CSC) for the scholarship (No. 201506630046) provided to the first author of this paper. The authors express their appreciation to Ms Xiaorui Hu (Donghua University) for technical assistance. We also gratefully acknowledge support from the MoE Innovation Team Project in Biological Fibres Advanced Textile Processing and Clean Production at Wuhan Textile University for the fabric sample preparations.

Author Contributions: Fengxin Sun and Zhiqiang Chen performed the experiments; Fengxin Sun, Zhiqiang Chen and Licheng Zhu analyzed the data; Zhaoqun Du and Xungai Wang supported the experiment; Fengxin Sun, Zhiqiang Chen and Maryam Naebe wrote the paper; Maryam Naebe conceived the idea and supervise the research. All authors discussed the results and approved the final manuscript.

Conflicts of Interest: The authors declare no conflict of interest.

References

1. Liu, K.; Yao, X.; Jiang, L. Recent developments in bio-inspired special wettability. *Chem. Soc. Rev.* **2010**, *39*, 3240–3255. [CrossRef] [PubMed]
2. Parker, A.R.; Lawrence, C.R. Water capture by a desert beetle. *Nature* **2001**, *414*, 33–34. [CrossRef] [PubMed]
3. Zheng, Y.; Bai, H.; Huang, Z.; Tian, X.; Nie, F.Q.; Zhao, Y. Directional water collection on wetted spider silk. *Nature* **2010**, *463*, 640–643. [CrossRef] [PubMed]
4. Ju, J.; Bai, H.; Zhengm, Y. A multi-structural and multi-functional integrated fog collection system in cactus. *Nat. Commun.* **2012**, *3*, 1247. [CrossRef] [PubMed]
5. Chen, Y.; Wang, L.; Xue, Y.; Zheng, Y.; Jiang, L. Bioinspired spindle-knotted fibers with a strong water-collecting ability from a humid environment. *Soft Matter* **2012**, *8*, 11450–11454. [CrossRef]
6. Darmanin, T.; Guittard, F. Superhydrophobic and superoleophobic properties in nature. *Mater. Today* **2015**, *18*, 273–285. [CrossRef]
7. Dai, X.; Imamura, R.; Liu, G.; Zhou, F. Effect of moisture transport on microclimate under T-shirts. *Eur. J. Appl. Physiol.* **2008**, *104*, 337–340. [CrossRef] [PubMed]
8. Rao, A.P.; Desai, N.V.; Rangarajan, R. Interfacially synthesized thin film composite RO membranes for seawater desalination. *J. Membr. Sci.* **1997**, *124*, 263–272.
9. Zeng, C.; Wang, H.; Zhou, H.; Lin, T. Heat Transfer in Directional Water Transport Fabrics. *Fibers* **2016**, *4*, 26. [CrossRef]
10. Li, Y. Perceptions of temperature, moisture and comfort in clothing during environmental transients. *Ergonomics* **2005**, *48*, 234–248. [CrossRef] [PubMed]
11. Wang, H.; Ding, J.; Dai, L.; Wang, X.; Lin, T. Directional water-transfer through fabrics induced by asymmetric wettability. *J. Mater. Chem.* **2010**, *20*, 7938–7940. [CrossRef]
12. Zhang, Y.; Barboiu, M. Dynameric asymmetric membranes for directional water transport. *Chem. Commun.* **2015**, *51*, 15925–15927. [CrossRef] [PubMed]
13. Wu, J.; Wang, N.; Wang, L.; Dong, H.; Zhao, Y.; Jiang, L. Unidirectional water-penetration composite fibrous film via electrospinning. *Soft Matter* **2012**, *8*, 5996–5999. [CrossRef]
14. Furstner, R.; Barthlott, W.; Neinhuis, C.; Walzel, P. Wetting and self-cleaning properties of artificial superhydrophobic surfaces. *Langmuir* **2005**, *21*, 956–961. [CrossRef] [PubMed]
15. Wang, H.; Fang, J.; Cheng, T.; Ding, J.; Qu, L.; Dai, L.; Wang, X.; Lin, T. One-step coating of fluoro-containing silica nanoparticles for universal generation of surface superhydrophobicity. *Chem. Commun.* **2008**, *7*, 877–879. [CrossRef] [PubMed]

16. Love, J.C.; Gates, B.D.; Wolfe, D.B.; Paul, K.E.; Whitesides, G.E. Fabrication and wetting properties of metallic half-shells with submicron diameters. *Nano Lett.* **2002**, *2*, 891–894. [CrossRef]
17. Jeyaprakash, J.D.; Samuel, S.; Ruhe, J. A facile photochemical surface modification technique for the generation of microstructured fluorinated surfaces. *Langmuir* **2004**, *20*, 10080–10085. [CrossRef] [PubMed]
18. Samuel, J.J.; Steger, R.; Birkle, G. Modification of micronozzle surfaces using fluorinated polymeric nanofilms for enhanced dispensing of polar and nonpolar fluids. *Anal. Chem.* **2005**, *77*, 6469–6474. [CrossRef] [PubMed]
19. Dorrer, C.; Ruehe, J. Wetting of silicon nanograss: From superhydrophilic to superhydrophobic surfaces. *Adv. Mater.* **2008**, *20*, 159–163. [CrossRef]
20. Wang, H.; Wang, X.; Lin, T. Unidirectional water transfer effect from fabrics having a superhydrophobic-to-hydrophilic gradient. *J. Nanosci. Nanotechnol.* **2013**, *13*, 839–842. [CrossRef] [PubMed]
21. Purcar, V.; Stamatin, I.; Cinteza, O. Fabrication of hydrophobic and antireflective coatings based on hybrid silica films by sol–gel process. *Surf. Coat. Technol.* **2012**, *206*, 4449–4454. [CrossRef]
22. Sarkar, M.K.; Bal, K.; He, F.; Fan, J. Design of an outstanding super-hydrophobic surface by electro-spinning. *Appl. Surf. Sci.* **2011**, *257*, 7003–7009. [CrossRef]
23. Ma, M.; Gupta, M.; Li, Z.; Zhai, L.; Gleason, K.K.; Cohen, R.E.; Rutledge, G.C. Decorated electrospun fibers exhibiting superhydrophobicity. *Adv. Mater.* **2007**, *19*, 255–259. [CrossRef]
24. Genzer, J.; Efimenko, K. Creating long-lived superhydrophobic polymer surfaces through mechanically assembled monolayers. *Science* **2000**, *290*, 2130–2133. [CrossRef] [PubMed]
25. Mates, J.E.; Bayer, I.S.; Palumbo, J.M.; Carroll, P.J.; Megaridis, C.M. Extremely stretchable and conductive water-repellent coatings for low-cost ultra-flexible electronics. *Nat. Commun.* **2015**, *6*, 8874. [CrossRef] [PubMed]
26. Tian, X.; Jin, H.; Sainio, J.; Ras, R.H.; Ikkala, O. Droplet and fluid gating by biomimetic janus membranes. *Adv. Funct. Mater.* **2014**, *24*, 6023–6028. [CrossRef]
27. Zeng, C.; Wang, H.; Zhou, H.; Lin, T. Directional water transport fabrics with durable ultra-high one-way transport capacity. *Adv. Mater. Interfaces* **2016**, *3*, 1600036. [CrossRef]
28. Naebe, M.; Denning, R.; Huson, M.; Cookson, P.G.; Wang, X. Ageing effect of plasma-treated wool. *J. Text. Inst.* **2011**, *102*, 1086–1093. [CrossRef]
29. Senthilkumar, P.; Karthik, T. Effect of argon plasma treatment variables on wettability and antibacterial properties of polyester fabrics. *J. Inst. Eng.* **2016**, *97*, 19–29. [CrossRef]
30. Wang, C.X.; Ren, Y.; Lv, J.C. In situ synthesis of silver nanoparticles on the cotton fabrics modified by plasma induced vapor phase graft polymerization of acrylic acid for durable multifunction. *Appl. Surf. Sci.* **2017**, *396*, 1840–1848. [CrossRef]
31. Kale, K.H.; Palaskar, S. Atmospheric pressure plasma polymerization of hexamethyldisiloxane for imparting water repellency to cotton fabric. *Text. Res. J.* **2011**, *81*, 608–620. [CrossRef]
32. Kwon, S.O.; Ko, T.J.; Yu, E.; Kimc, J.; Moon, M.M.; Park, C.H. Nanostructured self-cleaning lyocell fabrics with asymmetric wettability and moisture absorbency (part I). *RSC Adv.* **2014**, *4*, 45442–45448. [CrossRef]
33. Yim, J.H.; Rodriguez-Santiago, V.; Williams, A.A.; Gougousi, T.; Pappas, D.D.; Hirvonen, J.K. Atmospheric pressure plasma enhanced chemical vapor deposition of hydrophobic coatings using fluorine-based liquid precursors. *Surf. Coat. Technol.* **2013**, *234*, 21–32. [CrossRef]
34. Zhu, L.; Naebe, M.; Blanchonette, I.; Wang, X. Physical properties of novel co-woven-knitted fabrics. In Proceedings of the 89th Textile Institute World Conference, Wuhan, China, 2–6 November 2014; pp. 229–234.
35. Zhu, L.; Naebe, M.; Blanchonette, I.; Wang, X. Moisture transfer properties of bifacial fabrics. *Text. Res. J.* **2017**, *87*, 1096–1106. [CrossRef]
36. Zhu, L.; Wang, X.; Hinestroza, J.P.; Naebe, M. Determination of the porosity in a bifacial fabric using micro-computed tomography and three-dimensional reconstruction. *Text. Res. J.* **2017**. [CrossRef]
37. Chen, Z.; Dai, X.J.; Lamb, P.R.; du Plessis, J.; de Celis Leal, D.R.; Magniez, K.; Wang, X. Coating and functionalization of carbon fibres using a three-step plasma treatment. *Plasma Process. Polym.* **2013**, *10*, 1100–1109. [CrossRef]
38. Wan, A.; Dai, X.J.; Magniez, K.; du Plessis, J.; Yu, W.; Wang, W. Reducing the pilling propensity of wool knits with a three-step plasma treatment. *Text. Res. J.* **2013**, *83*, 2051–2059. [CrossRef]
39. Dai, X.J.; Chen, Y.; Chen, Z.; Lamb, P.R.; Li, L.H.; Plessis, J.D.; McCulloch, D.G.; Wang, G. Controlled surface modification of boron nitride nanotubes. *Nanotechnology* **2011**, *22*, 245–301. [CrossRef] [PubMed]

40. Du, Z.; Yu, W.; Zhou, T. Device and Method for Measuring Flexural Stiffness of Textile Fabric. China Patent CN101936856 B, 13 June 2012.
41. Du, Z.; Yu, W. A comprehensive handle evaluation system for fabrics: I. Measurement and characterization of mass and bending properties. *Meas. Sci. Technol.* **2007**, *18*, 3547. [CrossRef]
42. Zhang, C.; Zhao, M.; Wang, L.; Qu, L.; Men, Y. Surface modification of polyester fabrics by atmospheric-pressure air/He plasma for color strength and adhesion enhancement. *Appl. Surf. Sci.* **2017**, *400*, 304–311. [CrossRef]
43. Oktem, T.; Ayhan, H.; Seventekin, N.; Piskin, E. Modification of polyester fabrics by in situ plasma or post-plasma polymerisation of acrylic acid. *Colo. Technol.* **1999**, *115*, 274–279. [CrossRef]
44. Wang, C.; Qiu, Y. Study on wettability improvement and its uniformity of wool fabric treated by atmospheric pressure plasma jet. *J. Appl. Polym. Sci.* **2012**, *123*, 1000–1006. [CrossRef]
45. Naebe, M.; Cookson, P.G.; Rippon, J.; Brady, R.P.; Wang, X.; Brack, N.; Riessen, G.V. Effects of plasma treatment of wool on the uptake of sulfonated dyes with different hydrophobic properties. *Text. Res. J.* **2010**, *80*, 312–324. [CrossRef]
46. Teshima, K.; Sugimura, H.; Inoue, Y.; Takai, O.; Takano, A. Transparent ultra water-repellent poly(ethylene terephthalate) substrates fabricated by oxygen plasma treatment and subsequent hydrophobic coating. *Appl. Surf. Sci.* **2005**, *244*, 619–622. [CrossRef]
47. Molina, R.; Espinos, J.P.; Yubero, F.; Erra, P.; González-Elipeb, A.R. XPS analysis of down stream plasma treated wool: Influence of the nature of the gas on the surface modification of wool. *Appl. Surf. Sci.* **2005**, *252*, 1417–1429. [CrossRef]
48. Kan, C.; Chan, K.; Yuen, C.; Miao, M. Low temperature plasma on wool substrates: The effect of the nature of the gas. *Text. Res. J.* **1999**, *69*, 407–416. [CrossRef]
49. Yao, J.; Liu, Y.; Yang, S.; Liu, J. Characterization of secondary structure transformation of stretched and slenderized wool fibers with FTIR spectra. *J. Eng. Fibers Fabr.* **2008**, *3*, 22–31.
50. Muyonga, J.H.; Cole, C.G.B.; Duodu, K.G. Fourier transform infrared (FTIR) spectroscopic study of acid soluble collagen and gelatin from skins and bones of young and adult Nile perch (Lates niloticus). *Food Chem.* **2004**, *86*, 325–332. [CrossRef]
51. Li, H.F.; Dimitrijev, S.; Sweatman, D.; Harrison, H.B.; Tanner, P. Distribution and chemical bonding of N at NO nitrided SiC/SiO/sub 2/interface. In Proceedings of the 1998 Conference on Optoelectronic and Microelectronic Materials and Devices, Perth, Australia, 14–16 December 1998; pp. 164–166.
52. Jradi, K.; Daneault, C.; Chabot, B. Chemical surface modification of glass beads for the treatment of paper machine process waters. *Thin Solid Films* **2011**, *519*, 4239–4245. [CrossRef]
53. Ji, Y.Y.; Hong, Y.C.; Lee, S.H.; Kim, S.D.; Kim, S.S. Formation of super-hydrophobic and water-repellency surface with hexamethyldisiloxane (HMDSO) coating on polyethyleneteraphtalate fiber by atmosperic pressure plasma polymerization. *Surf. Coat. Technol.* **2008**, *202*, 5663–5667. [CrossRef]
54. Hu, J.; Li, Y.; Yeung, K.-W.; Wong, A.S.W.; Xu, W. Moisture Management Tester: A Method to Characterize Fabric Liquid Moisture Management Properties. *Text. Res. J.* **2005**, *75*, 57–62. [CrossRef]
55. Karahan, M.; Eren, R. Experimental investigation of the effect of fabric parameters on static water absorption in terry fabrics. *Fibres Text. East. Eur.* **2006**, *14*, 59–63.
56. Karahan, M. Experimental investigation of the effect of fabric construction on dynamic water absorbtion in terry fabrics. *Int. J. Radiat. Oncol. Biol. Phys.* **2007**, *46*, 1193–1197.
57. Yao, B.-G.; Li, Y.; Hu, J.-Y.; Kwok, Y.-L.; Yeung, K.-W. An improved test method for characterizing the dynamic liquid moisture transfer in porous polymeric materials. *Polym. Test.* **2006**, *25*, 677–689. [CrossRef]
58. Sun, F.; Asad, R.A.M.; Du, Z.; Yu, W.; Chen, N. Fuzzy comprehensive prediction of fabric stiffness handle based on quasi-three-point restraint test. *Fibers Polym.* **2015**, *16*, 1395–1402. [CrossRef]
59. Sun, D.; Stylios, G.K. Fabric surface properties affected by low temperature plasma treatment. *J. Mater. Proc. Technol.* **2006**, *173*, 172–177. [CrossRef]